https://doi.org/10.32604/zkg.2026.086486

ARTICLE

The recycling of waste mould plaster through low-temperature modification and properties

Zhong-jie Wang[1], Lian-xing Wang[2] and Chao-qiang Wang[3,*]
[1]School of Civil Engineering, Chongqing Jiaotong University, Chongqing, China
[2]CCCC Third Harbor Engineering (Xiamen) Ocean Engineering Co., Ltd., Xiamen, China
[3]School of Materials Science and Engineering, Chongqing Jiaotong University, Chongqing, China
*Corresponding Author: Chao-qiang Wang. Email: wcq598676239@126.com

Received: 05 June 2026; Accepted: 31 August 2026

ABSTRACT: To enhance the resource recovery of waste mold gypsum and improve its applicability in building materials, industrial waste gypsum was thermally treated at 160, 180, 200, and 220°C. The effects on mechanical performance, phase assemblage, microstructure, and environmental safety were systematically examined. Increasing the treatment temperature from 160 to 200°C markedly improved the 2 h flexural and compressive strengths, while a further increase to 220°C led to a decline. The optimum condition was 200°C for 6 h, at which the modified waste gypsum achieved a 2 h flexural strength of 2.8 MPa and a compressive strength of 6.0 MPa, meeting the Grade 2.0 strength requirements of ASTM C472-20. Phase analysis and XRD characterization showed that, after treatment at 200°C, gypsum dihydrate was largely dehydrated, with hemihydrate gypsum (31.5%) as the predominant phase and a substantial proportion of soluble anhydrite AIII (29.2%). SEM observations revealed that the 200°C sample possessed a more uniform crystal morphology and denser microstructure. TG-DSC and FTIR results demonstrated that the main dehydration process occurred within 100–150°C, with approximately 120°C identified as the characteristic conversion temperature. XRF confirmed that thermal modification did not fundamentally alter the bulk chemical composition, which remained dominated by the Ca-S-O system. The concentrations of Cu, As, Cd, Hg, and Pb were all low and met environmental safety requirements. Under the optimum condition, the process carbon emission was 7.63 kg CO_2-eq per batch, with a unit carbon emission of 3.81 kg CO_2-eq/kg and a carbon efficiency of 1.57, indicating a favorable balance between mechanical performance and environmental burden.

KEYWORDS: Waste gypsum; thermal modification; phase transformation; mechanical properties; carbon emission reduction

1 Introduction

Gypsum, primarily composed of calcium sulfate dihydrate ($CaSO_4 \cdot 2H_2O$), is one of the most widely used materials in the building and construction industry. However, the extensive extraction and production of gypsum have led to significant environmental concerns, particularly the accumulation of large quantities of waste gypsum [1, 2]. Such waste is often disposed of in landfills, resulting in land occupation, water contamination, and an increasing burden on waste management systems [3]. As the availability of high-quality natural gypsum resources continues to decline, the recycling and reuse of waste gypsum have become increasingly important. Effective recovery of waste gypsum can not only alleviate environmental pressure but also contribute to the development of a circular economy [4–6].

Although the recycling of waste gypsum has increased globally in recent years, marked regional disparities remain. In developed areas, particularly Europe and North America, waste gypsum has already been recycled at a comparatively high rate, and the recovered material is mainly reused in construction products and fertilizers [5, 7, 8]. By contrast, despite being the largest producer and consumer of gypsum worldwide, China still faces considerable obstacles in achieving high-value utilization of waste gypsum [9, 10]. China possessed abundant natural gypsum resources. Nevertheless, current recycling practices are still largely confined to low-end uses, such as soil improvement and landfill disposal, which results in substantial resource loss [11–13]. Therefore, further efforts should focus on promoting the high-value application of waste gypsum, especially by enhancing its properties for advanced building-material applications.

In industrial applications, gypsum materials are widely used not only in construction but also in mold

MATERIALS

manufacturing. Among them, beta-hemihydrate gypsum (β-$CaSO_4 \cdot 0.5H_2O$) is the most common type used in industrial gypsum molds because of its simple production process, low cost, and favorable molding performance [14–16]. β-Hemihydrate gypsum is typically produced by calcining natural gypsum under atmospheric pressure. Its relatively loose particle structure and large specific surface area provide good water absorption capacity and formability [16, 17]. In practical applications, gypsum-based mold materials are widely used in ceramic slip-casting molds because of their ease of shaping, low cost, and porous structure after hardening. In addition, gypsum materials have long been used in dental models and investment casting materials [18, 19]. Among these applications, slip casting in the ceramic industry is one of the most representative uses of gypsum molds [20]. This process relies on the porous structure and capillary suction of the gypsum mold to absorb liquid from the slurry into the mold interior, causing particles to deposit near the mold wall and gradually form a green body of a certain thickness. Consequently, the pore size distribution, porosity, and microstructure of the mold directly affect the casting rate and service performance of the mold. This forming mechanism has been widely applied in the manufacture of sanitary ceramics and other ceramic products with complex shapes [21].

However, during repeated use, the pore structure of gypsum molds gradually becomes blocked by fine-particle deposition, accompanied by a decline in water absorption capacity, deterioration in mechanical properties, and reduced dimensional accuracy. As a result, the service life of gypsum molds is limited, and periodic replacement is required [22]. Therefore, in continuous ceramic production, especially in the manufacture of sanitary ceramics, large amounts of waste mold gypsum are continuously generated. With the expansion of the ceramic and related building materials industries, both gypsum consumption and solid waste generation have attracted increasing attention. In the absence of efficient resource-recovery routes, these wastes are generally disposed of by stockpiling or landfilling, creating pressure on land use and environmental management systems [23].

Thermal modification is considered an important strategy for regulating the phase composition and service performance of gypsum [24, 25]. When heated, gypsum undergoes stepwise dehydration accompanied by phase transformation, and these changes are highly temperature dependent. Previous investigations have shown that heating in the approximate range of 80–180°C promotes the formation of hemihydrate gypsum, with β-hemihydrate gypsum generally being the predominant product under conventional atmospheric calcination conditions. With further temperature increase, the material may continue converting to soluble anhydrite III and anhydrite II. Excessively high temperatures can additionally cause severe cracking, structural densification, and sintering phenomena [24, 25]. In contrast, alpha-hemihydrate gypsum (α-$CaSO_4 \cdot 0.5H_2O$) is typically prepared by hydrothermal methods or salt-solution-mediated hydrothermal crystallization, and its crystal morphology and mechanical properties differ markedly from those of β-hemihydrate gypsum [26–28]. These temperature-induced phase transitions and microstructural changes further affect the strength, pore structure, hydration behavior, and durability of gypsum-based materials. Therefore, thermal modification is regarded as one of the key process routes for improving the regeneration performance of waste gypsum and achieving its high-value utilization [29].

To further improve the performance of gypsum materials, various synergistic physical and chemical modification approaches have been proposed [29, 30]. Among them, enhancement of mechanical properties has been one of the most extensively studied directions. By optimizing calcination conditions and incorporating cement, mineral admixtures, water reducers, fibers, and other additives, it is possible to reduce water demand, optimize crystal packing and pore structure, and thereby improve the flexural strength, compressive strength, and durability of gypsum-based materials [31]. For instance, superplasticizers can facilitate the development of a more compact crystal network, thereby enhancing both strength and water resistance, whereas fiber incorporation is effective in reducing brittle fracture and improving the overall mechanical reliability of gypsum composites [30, 31]. Nevertheless, poor water resistance remains a major bottleneck restricting the high-value application of waste gypsum. Existing studies have shown that combining thermal modification with organic waterproofing agents, fiber/polymer modification, or cement-slag composite systems can markedly enhance the water resistance of gypsum products. This effect is generally associated with lower porosity, reduced capillary absorption, and the formation of more stable hydration phases, which collectively broaden the applicability of these materials in construction engineering [29].

Previous studies have demonstrated the feasibility of environmental and safety assessment for gypsum-based industrial-waste systems. For example, Wang et al. [32] investigated a red-mud-modified phosphogypsum composite cementitious material and systematically evaluated the associated heavy-metal environmental and human-health risks. However, such studies have mainly focused on phosphogypsum-based multi-component cementitious systems, whereas the regeneration of end-of-life industrial mold gypsum through direct low-temperature thermal treatment has received comparatively limited attention. In particular, the relationships among thermal-treatment conditions, phase transformation, mechanical recovery, process-related carbon

burden, and environmental safety remain insufficiently understood for waste mold gypsum.

Therefore, this study investigates waste mold gypsum obtained directly from an industrial source and systematically examines its thermal regeneration within the range of 160–220°C. The specific contribution of this work is to link dehydration-induced phase evolution and microstructural reconstruction with mechanical performance, while further incorporating process carbon emissions, carbon efficiency, and heavy-metal risk assessment into an integrated evaluation framework. This approach provides a material- and process-specific basis for identifying technically effective and environmentally acceptable conditions for the high-value utilization of industrial waste mold gypsum.

2 Materials and methods

2.1 Raw materials

The waste gypsum investigated in this work was collected from an industrial source in Chongqing, China. As illustrated in Figure 1, the waste gypsum was in lump form and therefore required crushing and screening prior to thermal modification. Analysis of the sample's XRD pattern reveals a strongest diffraction peak at approximately $2\theta = 11.8^{\circ}$, with distinct characteristic peaks also present at 20.9°, 23.6°, 29.3°, 31.3° and 33.5°. According to the locations of these diffraction peaks and their relative intensities, gypsum ($CaSO_4 \cdot 2H_2O$) was identified as the dominant crystalline constituent of the sample. Furthermore, the absence of dominant main peaks characteristic of impurities such as quartz in the diffraction pattern indicates that the sample is predominantly composed of the gypsum phase and exhibits good crystallinity.

2.2 Experimental methods

2.2.1 Sample preparation and strength testing

First, a hydraulic press is used to break large chunks of waste gypsum into smaller pieces; next, a crusher is used to further break these pieces into particles with a diameter of less than 18 mm. Finally, the crushed waste gypsum was ground and sieved to obtain a fine granules passing through a 3 mm sieve prior to thermal modification. It should be noted that the value of approximately 3 mm refers to the nominal upper size limit of the bulk ground powder used for calcination and specimen preparation, rather than the particle size measured by the particle size distribution test. Temperature treatment was carried out using an oven (XMTA-500T) with a heating rate of 5 °C/min and holding times of 4 and 6 h. These two holding times were selected because existing research indicates that the extent of phase transformation in gypsum is sensitive to holding time, with properties undergoing significant changes within a few hours [33]. Furthermore, excessively long heat treatment times significantly increase energy consumption and costs, which is not conducive to the widespread adoption of the technology; in industrial gypsum calcination processes, the residence time of the material is typically on the order of several hours (http://innogyps.com/gypsum_calcination.php). Finally, based on exploratory experiments conducted prior to the formal trials, it was found that holding times shorter than 4 h resulted in incomplete dehydration and unstable performance, whilst holding times exceeding 6 h led to an overly gradual increase in strength. Natural cooling in an air environment; sample spread thickness ≤3 cm; 2 kg per batch; three parallel samples per group. Test specimens for strength testing measured 40 mm × 40 mm × 160 mm, with a water-to-gypsum ratio of 0.45. Curing conditions were 95% relative humidity and 20°C, with a curing time of 2 h.

2.2.2 Characterization methods

(1) Heavy metal content

Heavy metal concentrations were determined by inductively coupled plasma mass spectrometry (ICP-MS) at Scientific Compass (Hangzhou,

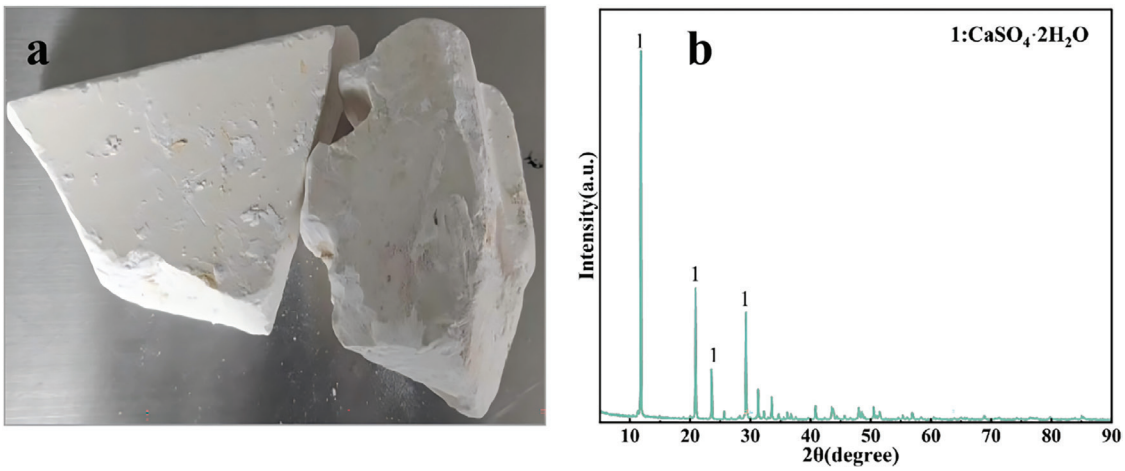


Figure 1 Characteristics of the raw waste mold gypsum: (a) Appearance of the waste gypsum; (b) XRD pattern

China). Prior to analysis, the solid samples were dried, homogenized, finely ground, and passed through a 200-mesh sieve. Approximately 0.20 g of each sample was accurately weighed and transferred into a digestion vessel. The samples were subjected to acid digestion using concentrated HNO_3, with H_2O_2 added when necessary to facilitate complete oxidation of the sample matrix. Microwave-assisted digestion was performed until a clear digestion solution was obtained. After cooling to room temperature, the digested solutions were quantitatively transferred into volumetric flasks and diluted to an appropriate final volume with ultrapure water. The resulting solutions were maintained under weakly acidic conditions and contained no visible suspended particles or insoluble residues.

The concentrations of the target heavy metals were determined using an inductively coupled plasma mass spectrometer (NexION 300X, PerkinElmer, USA). Prior to measurement, the digested solutions were appropriately diluted to ensure that the concentrations of the target elements fell within the calibration range. Multi-element standard solutions were serially diluted with ultrapure water and acidified with HNO_3 to establish external calibration curves. Reagent blanks were analyzed simultaneously to correct for background contamination introduced during sample preparation and instrumental analysis.

The concentrations of heavy metals in the original solid samples were calculated from the measured concentrations in the digestion solutions according to Eq. (1):

$$C = \frac{(C_m - C_b) \times V \times D}{m} \quad (1)$$

where (C) is the concentration of the target element in the original sample (mg kg^{-1}), (C_m) is the measured concentration of the element in the digestion solution (mg L^{-1}), (C_b) is the corresponding concentration in the reagent blank (mg L^{-1}), (V) is the final volume of the digestion solution (L), (D) is the dilution factor, and (m) is the dry mass of the sample (kg). Heavy metal concentrations were expressed on a dry-weight basis.

(2) PSD and XRD

X-ray diffraction (XRD) patterns were obtained using a Rigaku Ultima IV X-ray diffractometer (Rigaku Corporation, Japan) with Cu Kα radiation λ = 1.5406Å. The XRD data were collected in the 2θ range of 10–80° with a step size of 0.02° and a scanning rate of 5° min^{-1}. The instrument was operated at 40 kV and 40 mA, and the measurements were carried out at room temperature under ambient conditions. Particle size distribution (PSD) was measured using a Malvern Zetasizer Nano ZS (dynamic light scattering, DLS) after dispersing the sample in deionized water and ultrasonic treatment for 10 min. Z-average, PDI, and hydrodynamic diameter were recorded.

PSD analysis was conducted on representative sub-samples of the thermally modified waste gypsum powders. Before measurement, the powder sub-samples were re-dispersed in deionized water and ultrasonicated to reduce loose agglomeration. Therefore represent the hydrodynamic particle/agglomerate size of the re-dispersed and ultrasonicated sub-samples, rather than the millimetre-scale size of the bulk ground powder prepared before thermal modification.

(3) SEM-EDS

The microstructural features and elemental distribution of the gypsum samples were examined using a ZEISS Sigma 300 scanning electron microscope (Germany) equipped with an energy-dispersive spectroscopy (EDS) system.

(4) FTIR

Changes in the functional groups of gypsum before and after thermal treatment were analyzed using a Thermo Fisher Scientific Nicolet iS20 Fourier-transform infrared spectrometer.

(5) TG-DSC

Thermal behavior of the samples was investigated using a Mettler TGA/DSC instrument (Switzerland) over the range of 30–250°C at a heating rate of 5 °C/min.

(6) Three-phase analysis

A Yaguan gypsum four-phase analyzer (CS-90GLN) was used for three-phase analysis of the samples.

2.3 Methods for assessing heavy metal risks

2.3.1 Single-factor index method

The single-factor pollution index method is commonly used to assess environmental contamination and provides a basis for further comprehensive evaluation. It estimates the pollution level of each heavy metal by relating its measured concentration in the sample to the corresponding reference value, thus indicating its potential environmental impact. The relevant formula is given in Eq. (2).

$$P_i = C_i / S_i \quad (2)$$

To ensure consistency and comparability, the definitions and values of all parameters used in this study were adopted from previous literature [34, 35].

2.3.2 Potential ecological risk method

Potential ecological risk assessment is one of the most commonly used approaches for characterizing the environmental hazards of heavy metals. This method combines the contamination level of each element, expressed as the ratio between measured concentration and reference value, with its toxic-response factor to quantify the possible ecological threat posed by different heavy metals. Because it allows the integrated evaluation of ecological risks arising from multiple pollutants, it has been widely employed in environmental

assessment research. The detailed formula is shown in Eq. (3).

$$RI = \sum_{i=1}^{n} E_r^i = \sum_{i=1}^{n} T_r^i \times C_f^i = \sum_{i=1}^{n} T_r^i \times \frac{C_s^i}{C_O^i} \quad (3)$$

2.3.3 Geoaccumulation index method

In the geoaccumulation index method, a background correction coefficient is incorporated into the evaluation, so that both natural geological effects on elemental concentrations and heavy metal accumulation resulting from human activities can be considered simultaneously. As this method is useful for tracing pollution sources and assessing their environmental significance, it was applied in this work to evaluate the potential environmental impacts associated with the resource recovery and utilization of waste gypsum. The relevant equation is shown in Equation (4).

$$I_{geo} = \log_2\left(\frac{C_n}{1.5 \times B_n}\right) \quad (4)$$

2.3.4 Human health risk assessment

Waste gypsum contains trace heavy metal elements that may affect not only the soil environment but also human health through multiple exposure pathways. Therefore, a human health risk assessment was conducted in this study. The assessment was based on the Chinese national standard Technical guidelines for risk assessment of soil contamination of land for construction (HJ 25.3-2019) [36], the health risk assessment model proposed by the US Environmental Protection Agency (Risk Assessment Guidance for Superfund (RAGS) Volume III: Part A-US EPA (https://www.epa.gov/risk/risk-assessment-guidance-superfund-rags-volume-iii-part)), and relevant literature. Non-carcinogenic and carcinogenic risks associated with Cu, As, and Pb in waste gypsum were evaluated. The major exposure pathways considered included oral ingestion, inhalation, and dermal contact. By comprehensively considering these pathways, the potential human health risks posed by heavy metals in waste gypsum were assessed. The calculation formulas and parameter definitions used in this study were adopted from previous studies [34, 35].

2.4 Carbon emission assessment method

To evaluate the environmental performance of the thermal modification process, a carbon emission assessment was conducted based on the electricity consumption of the heating treatment. The carbon footprint of each treatment condition was calculated using the electricity consumed during thermal modification and the corresponding grid emission factor. The carbon emissions were expressed as kg CO_2-eq per kg of modified waste gypsum. The calculation is shown in Eqs. (5) and (6):

$$E = P \times t \quad (5)$$

$$CF = E \times EF_{elec} \quad (6)$$

where CF is the process carbon emission (kg CO_2-eq), and EF_{elec} is the electricity carbon footprint factor (kg CO_2-eq/kWh). In this study, the 2024 national average electricity carbon footprint factor of China, 0.5777 kg CO_2-eq/kWh, was adopted for calculation. To express the carbon burden of the process on a mass basis, the unit carbon emission of modified waste gypsum was calculated using Eq. (7):

$$CF_{unit} = \frac{CF}{m} \quad (7)$$

where CF_{unit} is the unit carbon emission (kg CO_2-eq/kg), and m is the mass of waste gypsum treated in one batch (kg).

In addition, in order to evaluate the balance between mechanical performance and environmental cost, a carbon efficiency index was defined as the ratio of compressive strength to unit carbon emission, as shown in Eq. (8):

$$CE = \frac{\sigma_c}{CF_{unit}} \quad (8)$$

where CE is the carbon efficiency, and σ_c is the compressive strength of the modified waste gypsum (MPa). A higher CE value indicates that a higher mechanical performance was achieved per unit carbon emission.

3 Results and discussion

3.1 Analysis of physical properties

3.1.1 Flexural and compressive strength

Figure 2 shows that the early mechanical performance of waste gypsum was strongly affected by both thermal treatment temperature and holding time. For the 4 h treatment series, the flexural strength increased from 2.0 MPa at 160°C to 2.4 MPa at 200°C, while the compressive strength increased from 3.1 MPa to 5.1 MPa over the same temperature range. For the 6 h treatment series, the flexural strength increased from 1.9 MPa at 160°C to 2.8 MPa at 200°C, whereas the compressive strength increased from 4.4 MPa to 6.0 MPa. These results indicate that increasing the treatment temperature from 160 to 200°C promoted the dehydration of gypsum and favored the formation of hemihydrate gypsum, thereby improving early-age strength [24, 25]. However, further heating to 220°C caused a decline or stagnation in strength. This suggests that an excessively high treatment temperature was unfavorable for early strength development, probably because part of the hemihydrate phase was further transformed

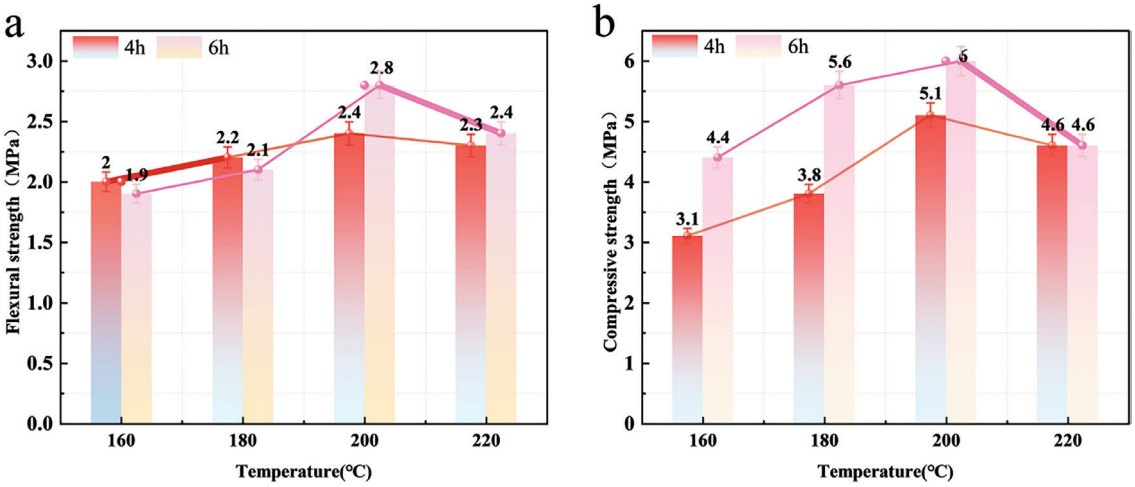


Figure 2 (a) Flexural strength; (b) Compressive strength

into less reactive anhydrite, accompanied by local structural defects.

The effect of holding time on flexural strength was temperature-dependent rather than consistently positive across the whole temperature range. At 160 and 180°C, the flexural strength of the 6 h samples was slightly lower than that of the 4 h samples, indicating that prolonging the holding time at relatively low temperatures did not further improve flexural performance. In contrast, at 200 and 220°C, the 6 h samples exhibited higher flexural strength than the corresponding 4 h samples. In particular, at 200°C, the flexural strength increased from 2.4 MPa for 4 h treatment to 2.8 MPa for 6 h treatment, and the compressive strength also reached the maximum value of 6.0 MPa. This indicates that, under an appropriate treatment temperature, extending the holding time to 6 h facilitated more complete phase transformation and contributed to the formation of a denser microstructure. This duration range aligns with the reported processing time of 2–24 h in the literature, which enables sufficient phase transition of gypsum [33, 37]. The physical strength tests were conducted with reference to ASTM C472-20 [38]. The resulting strength values were further compared with the strength-grade criteria listed in Table 1. Under the optimum thermal treatment condition of 200°C for 6 h, the modified waste gypsum reached a 2 h flexural strength of 2.8 MPa and a compressive strength of 6.0 MPa. These results indicate that the sample met the overall Grade 2.0 strength requirements, while its compressive strength reached the Grade 3.0 threshold.

Table 1 Strength requirements of calcined gypsum

Level	2 h strength/MPa	
	Flexural	Compressive
4.0	≥4.0	≥8.0
3.0	≥3.0	≥6.0
2.0	≥2.0	≥4.0

The compressive strength was significantly higher than the flexural strength, which is consistent with the typical behavior of hardened gypsum. Its microstructure is composed of interwoven needle-like crystals that remain relatively stable under compressive stress but are more sensitive to tensile and bending stresses because the intercrystalline bonding interfaces are more susceptible to failure under such loading conditions [39, 40]. This finding suggests that, if the modified gypsum is intended for load-bearing applications or applications requiring improved toughness, additional strengthening strategies, such as fiber reinforcement or polymer modification, should be considered to improve its flexural performance.

According to the phase transformation behavior of gypsum, the temperature increase from 160 to 200°C primarily promoted the partial dehydration of calcium sulfate dihydrate in the waste gypsum, resulting in the formation of hemihydrate gypsum with high cementitious activity. At 200°C, a balance between phase transformation and microstructural optimization was achieved, leading to the highest strength. When the temperature exceeded 200°C, the more reactive hemihydrate gypsum likely began to transform into soluble anhydrite (AIII), accompanied by reduced hydration activity, which in turn caused a decrease in early strength. It should be noted that although the AIII phase formed at 220°C can rehydrate upon contact with water, its rapid moisture adsorption from the air during storage may lead to partial pre-hydration and reduced effective reactivity, contributing to the observed strength decline. These results provide important experimental evidence for determining the processing parameters for waste gypsum recycling. Specifically, the modification temperature is recommended to be controlled at around 200°C, with an appropriately prolonged holding time (e.g., 6 h), in order to obtain a highly active gypsum-based

cementitious material. Under such optimized conditions, the modified waste gypsum shows promise for use in products such as gypsum blocks and plastering mortars, thereby enabling its high-value utilization.

Based on the flexural and compressive strength results, the optimal modification condition for waste gypsum in this study was determined to be 200°C for 6 h. To further clarify the reasons for this superior performance, detailed microstructural characterization of the optimally modified sample was subsequently conducted.

3.1.2 Three-phase analysis of gypsum

The three-phase analysis results shown in Figure 3 correspond to the optimally modified waste gypsum sample treated at 200°C for 6 h. The measured contents of hemihydrate gypsum (HH), dihydrate gypsum (DH), and soluble anhydrite (AIII) were 31.5%, 19.6%, and 29.2%, respectively, corresponding to a combined content of 80.3%. These values represent the individual mass fractions of the three target gypsum phases relative to the total sample mass and were not normalized to 100%. Therefore, the remaining fraction (approximately 19.7%) is attributed to components not included in the three-phase calculation, including other non-target mineral or calcium sulfate phases and inert impurities present in the industrial waste gypsum.

It should be noted that C2 and D2 in Figure 3 are not additional gypsum phases, but intermediate testing parameters generated by the gypsum phase composition analyzer. C2 represents the hydration-induced mass increment after the sample is mixed with distilled water, which is associated with the hydration reaction of active calcium sulfate phases such as HH and AIII. D2 represents the mass-loss fraction during high-temperature drying, mainly reflecting dehydration-related mass loss from DH and other volatile components. These two parameters are used by the built-in calculation model of the instrument to derive the final phase composition of HH, DH, and AIII.

Based on the phase contents shown in Figure 3, the combined proportion of the main active phases HH and AIII was 60.7% (31.5% + 29.2%). The relatively high proportion of HH and AIII indicates that thermal treatment at 200°C for 6 h effectively promoted the dehydration of dihydrate gypsum and generated active calcium sulfate phases. These phases are beneficial for subsequent hydration and early strength development, which is consistent with the mechanical performance of the optimally modified sample [40, 41].

3.2 SEM-EDS

To further elucidate the effects of thermal modification at different temperatures on the microstructure and elemental distribution of waste gypsum, the samples were characterized by SEM coupled with EDS.

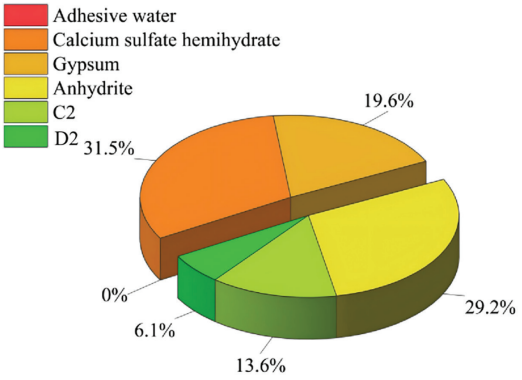


Figure 3 Analysis results of gypsum phase components

3.2.1 Microstructural morphology after modification at different temperatures

As shown in Figure 4, the SEM micrographs reveal clear differences in the microstructure of waste gypsum under different thermal modification temperatures.

At 160°C, the particles exhibit irregular shapes with loosely packed structures. Numerous voids and microcracks are observed between particles, indicating relatively poor structural compaction. The crystal boundaries are not clearly developed, suggesting that dehydration of gypsum is still limited at this stage.

When the temperature increases to 180°C, more defined crystal morphologies begin to appear. Some particles show plate-like or short columnar features, and partial crystal growth can be observed. However, the overall structure remains relatively loose, and interparticle pores are still widely distributed, indicating an intermediate stage of phase transformation.

At 200°C, the microstructure becomes significantly more compact. The particles are closely packed, crystal boundaries are clearer, and the number of visible pores is markedly reduced. Well-developed crystal facets and interlocking structures can be observed, suggesting a more complete transformation to hemihydrate gypsum and a denser microstructural arrangement.

When the temperature is further increased to 220°C, local fragmentation and agglomeration of particles are observed. In addition, microcracks and uneven pore structures appear in some regions, indicating structural instability possibly caused by excessive dehydration and partial phase transition. Compared with the 200°C sample, the overall microstructure becomes less uniform.

Overall, the SEM results show a gradual evolution from a loose and irregular structure (160–180°C) to a dense and well-structured morphology (200°C), followed by partial deterioration at excessive temperature (220°C).

3.2.2 Microstructure after secondary hydration

Figure 5 presents the SEM images of the modified gypsum samples after secondary hydration. After hydration, a large number of needle-like

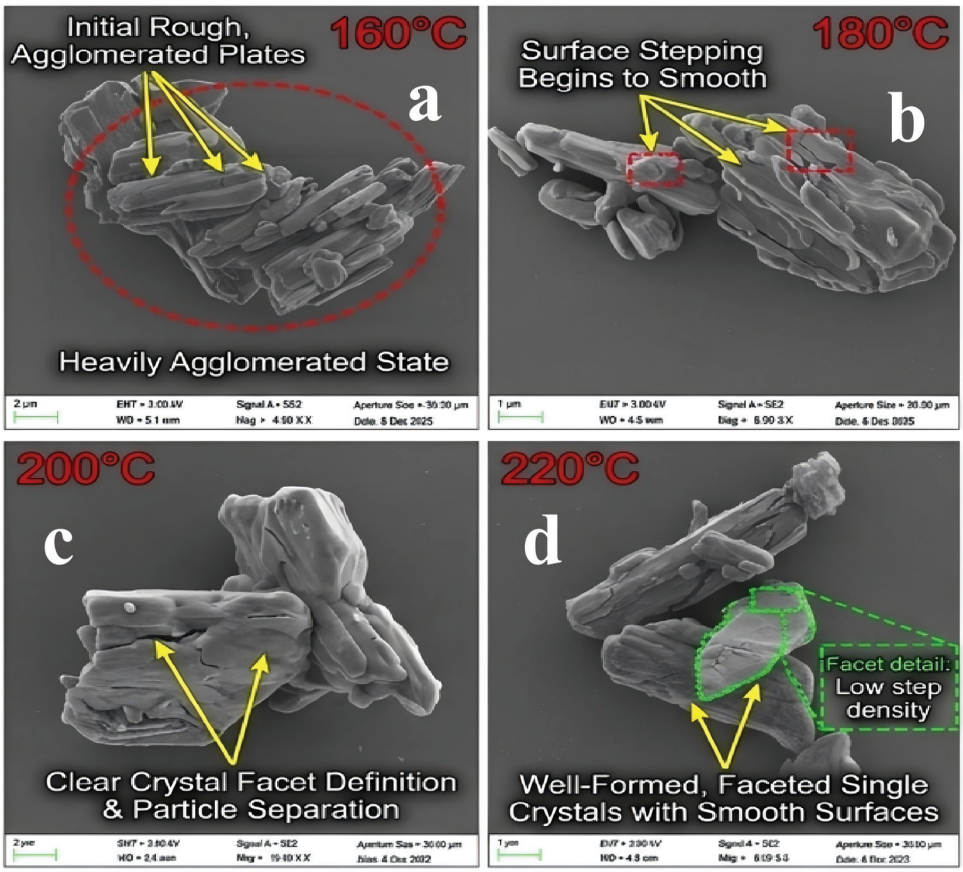


Figure 4 SEM micrographs of waste gypsum after thermal modification at different temperatures: (a) 160°C; (b) 180°C; (c) 200°C; (d) 220°C

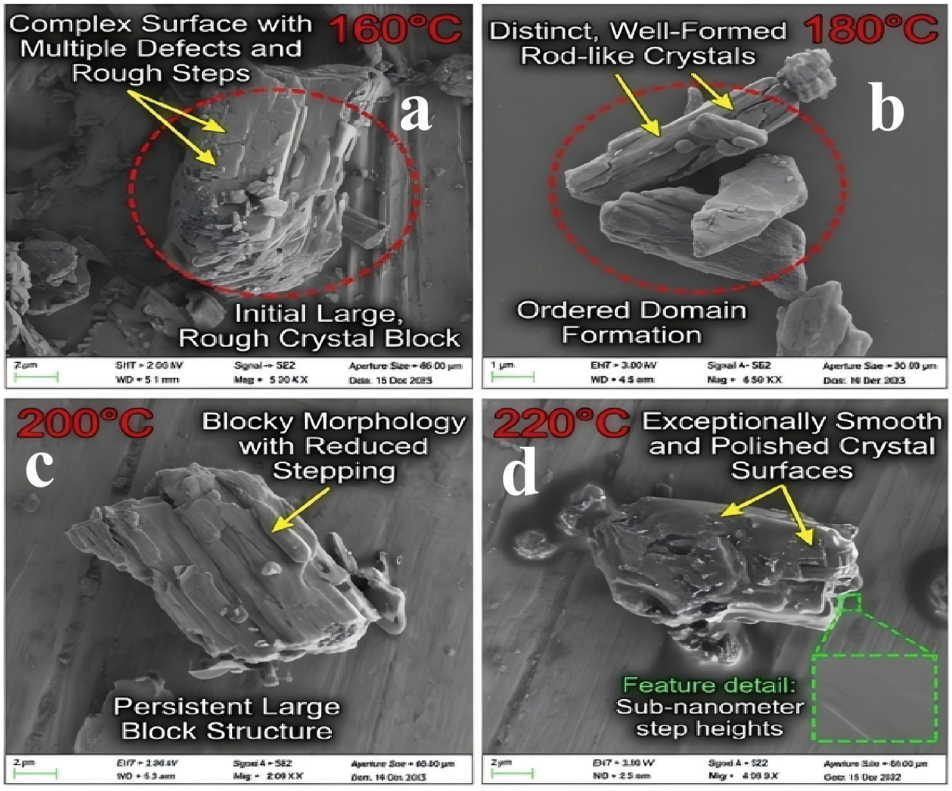


Figure 5 SEM micrographs of waste gypsum after secondary hydration at different temperatures: (a) 160°C; (b) 180°C; (c) 200°C; (d) 220°C

and columnar crystals can be clearly observed. These crystals are randomly interwoven to form a three-dimensional network structure, which is a typical morphology of hydrated calcium sulfate phases. For samples treated at 200°C, the hydrated crystals appear more densely packed, with a higher degree of interlocking between needle-like structures. This results in a more continuous and compact network morphology, which is consistent with the higher mechanical strength observed in the corresponding samples. In contrast, samples treated at lower temperatures show relatively fewer hydration products and a looser crystal network. For samples treated at 220°C, the crystal growth appears less uniform, with some discontinuous regions in the network structure, which may be related to reduced hydration activity after excessive thermal treatment. Overall, the secondary hydration morphology further confirms that the 200°C treated sample exhibits the most developed and compact crystal network.

3.2.3 EDS elemental composition analysis

Figures 6 and 7 present the EDS spectra of the thermally modified samples and the hydrated samples, respectively. As shown in the spectra, the dominant elements in both states were Ca, S, and O, corresponding to the basic composition of calcium sulfate ($CaSO_4$). This indicates that thermal modification and subsequent hydration mainly altered the hydration state and crystal structure of gypsum, rather than the elemental composition of the Ca-S-O framework [42].

In terms of peak intensity, the thermally modified samples exhibited distinct characteristic peaks for Ca, S, and O, with the peaks of Ca and S being particularly prominent, reflecting the relatively stable calcium sulfate structure and the concentrated distribution of these elements in the samples. In comparison, the hydrated samples still showed Ca, S, and O as the major constituent elements, but certain changes in peak intensity were observed. In particular, the signal intensity of O was relatively enhanced, whereas the peak intensities of Ca and S were slightly reduced or became less pronounced. This phenomenon may be associated with the incorporation of water molecules into the crystal structure during hydration, which increased the relative proportion or detectable signal of oxygen in the system.

In addition, as the hydration reaction proceeded, hemihydrate gypsum was reconverted into dihydrate gypsum, accompanied by the formation of an interwoven crystal structure. The coexistence of different phases within the EDS detection area may also have caused local variations in elemental signal intensity. Nevertheless, the overall elemental composition remained essentially stable. This further confirms that the thermal modification and hydration processes mainly affected the crystal structure and hydration state of gypsum, without fundamentally changing its elemental composition.

Minor signals of trace elements such as Cu, Pb, and As were also detected in the spectra. Their low peak intensities indicate that these elements were present only in small amounts, most likely originating from impurity phases in the original waste gypsum. Because their signals were weak and no obvious enrichment regions were observed, their influence on the microstructure and mechanical properties of the material was considered to be limited.

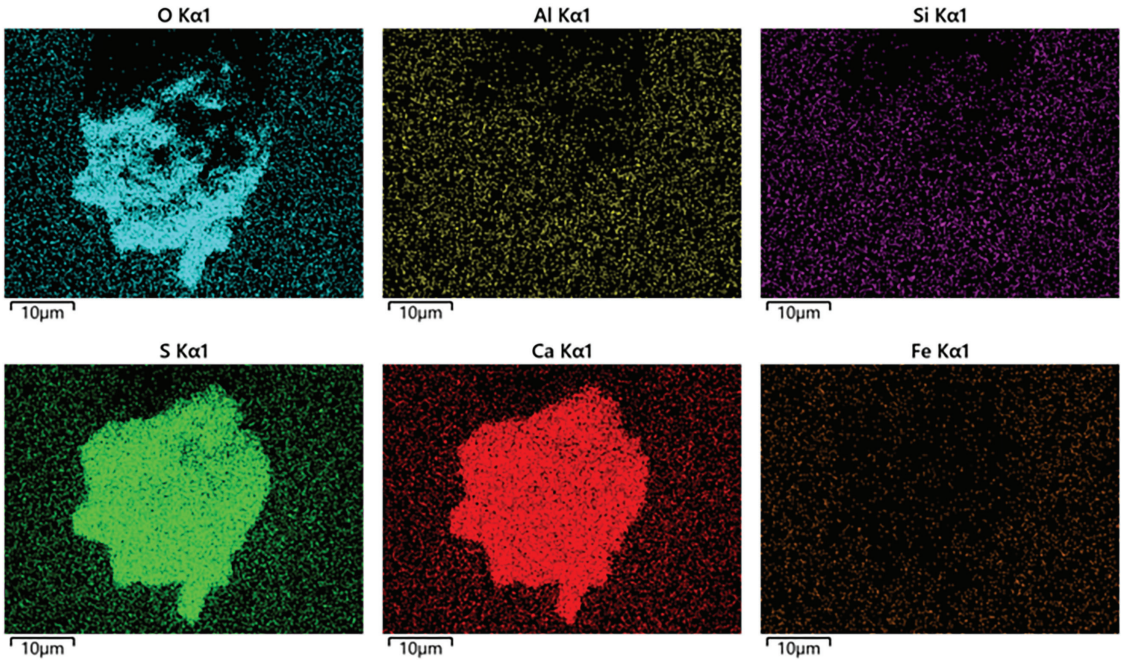


Figure 6 Heavy metal energy spectrum (thermal modification)

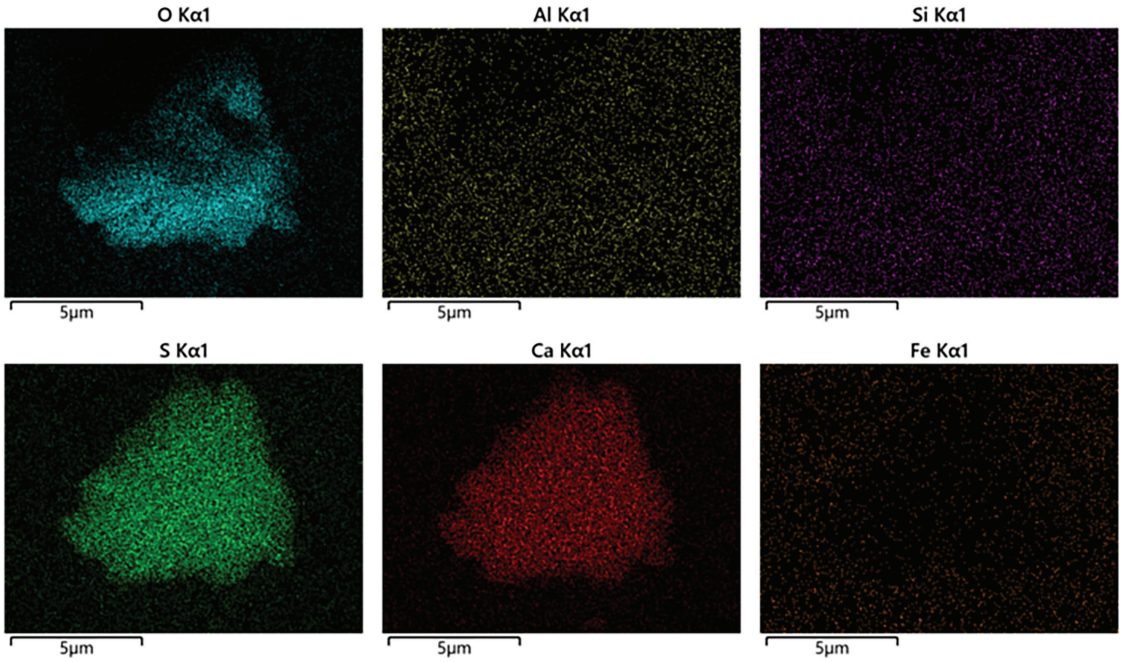


Figure 7 Heavy metal energy spectrum (secondary hydration)

3.2.4 Elemental distribution characteristics

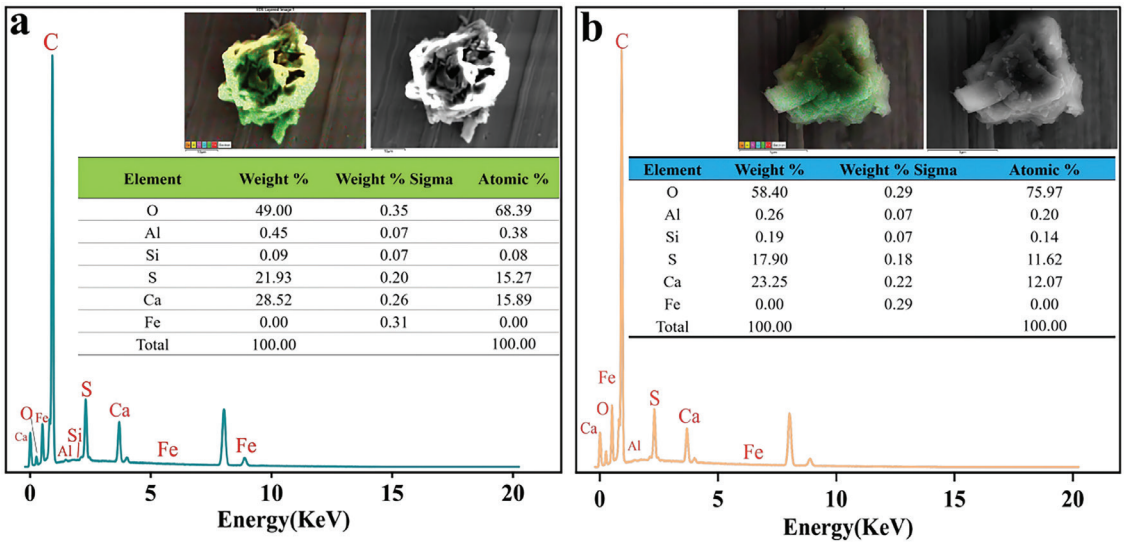
Figure 8 presents a comparison of the elemental mapping results of the thermally modified sample and the hydrated sample. As shown in the figure, the distributions of Ca, S, and O were relatively uniform, and no obvious elemental segregation was observed, indicating that the modification process did not lead to uneven elemental distribution within the samples.

At the same time, the signals of heavy metal elements were very weak, further suggesting that their contents in the samples were low. This result is consistent with the heavy metal concentration data subsequently obtained by ICP-OES, confirming that no significant risk of heavy metal enrichment was introduced during the thermal modification and resource utilization of the waste gypsum.

3.3 Particle size distribution and XRD analysis

X-ray diffraction was employed to examine how thermal modification at different temperatures affected the phase composition of waste gypsum. The samples treated at 160, 180, 200, and 220°C were analyzed, and the results are presented in Figure 9.

The PSD results in Figure 9 were obtained from representative sub-samples after re-dispersion



Element	Weight %	Weight % Sigma	Atomic %
O	49.00	0.35	68.39
Al	0.45	0.07	0.38
Si	0.09	0.07	0.08
S	21.93	0.20	15.27
Ca	28.52	0.26	15.89
Fe	0.00	0.31	0.00
Total	100.00		100.00

Element	Weight %	Weight % Sigma	Atomic %
O	58.40	0.29	75.97
Al	0.26	0.07	0.20
Si	0.19	0.07	0.14
S	17.90	0.18	11.62
Ca	23.25	0.22	12.07
Fe	0.00	0.29	0.00
Total	100.00		100.00

Figure 8 (a) The energy spectrum of thermal modification; (b) The energy spectrum of secondary hydration

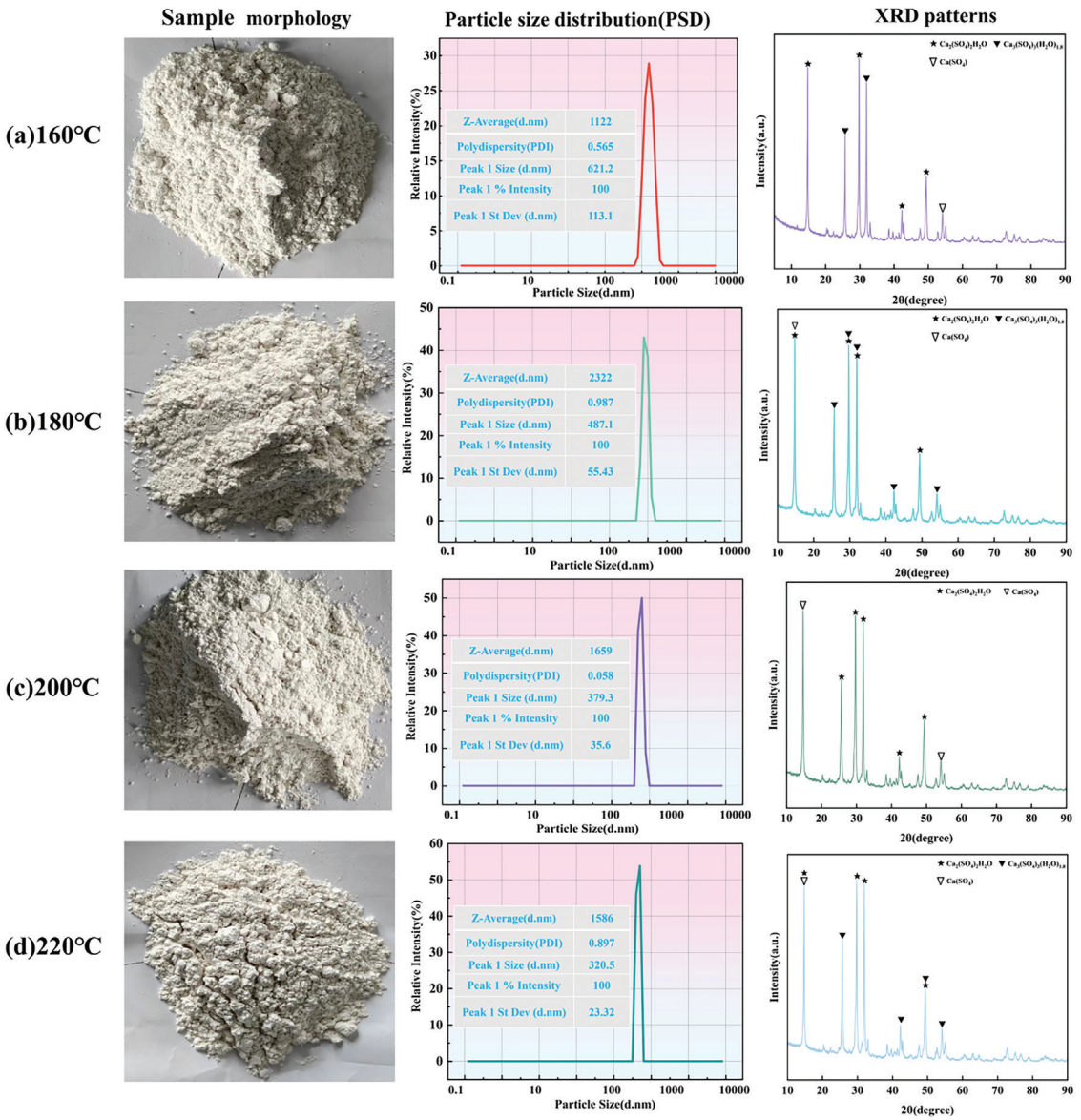


Figure 9 Gypsum powder, particle size distribution data and XRD images following treatment at different temperatures: (a) 160°C; (b) 180°C; (c) 200°C; (d) 220°C

and ultrasonication, rather than from direct measurement of the bulk ground powder. Therefore, the Z-average values in the range of approximately 1100–2300 nm should be interpreted as the hydrodynamic size of dispersed fine particles or residual agglomerates in suspension. These values are not directly comparable with the approximately 3 mm bulk grinding size described in Section 2.2.1, which only indicates the nominal upper size limit of the powder prepared for thermal modification and specimen preparation. The PSD results are used here mainly to compare the relative dispersion and agglomeration characteristics of the thermally modified samples. With increasing treatment temperature, the particle/agglomerate size distribution changed in a temperature-dependent manner, reflecting the combined effects of dehydration, fragmentation, and local agglomeration during calcination. At 200°C, the distribution was relatively concentrated, suggesting a more homogeneous dispersed powder system, which may be beneficial for water demand, particle packing, and subsequent strength development. When the temperature was further increased to 220°C, excessive dehydration and local agglomeration may have resulted in a less favorable particle arrangement. The formation of AIII at this temperature is consistent with the FTIR observation of increased –OH absorption, which originates from surface-adsorbed moisture on the hygroscopic AIII rather than from retained structural water. These PSD observations, together with the XRD results, support the conclusion that 200°C was the most suitable modification temperature in this study.

As shown in the figure, the modification temperature had a decisive influence on the final phase composition of the waste gypsum. Under

the 160°C treatment condition, diffraction peaks corresponding to gypsum, bassanite, and anhydrite could be clearly identified in the XRD pattern. Since this temperature is close to the onset of dehydration of gypsum, the results indicate that dehydration had already begun but remained incomplete. Therefore, the material remained composed of unconverted gypsum, transitional dehydration products, and a small proportion of anhydrite, with an overall low degree of crystallinity.

When the temperature increased to 180°C, the phase composition changed noticeably. The diffraction peaks of bassanite became more evident, while the peaks of gypsum and anhydrite were still present. This suggests that the dehydration process continued and generated intermediate hydrated phases with different crystallographic characteristics. Compared with the sample treated at 160°C, the overall peak intensity and sharpness were enhanced, implying that the crystallinity of the newly formed phases increased with rising treatment temperature and that the phase transformation proceeded more thoroughly.

A pronounced change in the XRD pattern was observed for the sample modified at 200°C. The diffraction peaks of bassanite became dominant, accompanied by distinct diffraction peaks of anhydrite. Meanwhile, the peaks of intermediate phases almost disappeared. These phase characteristics indicate that, at this temperature, the waste gypsum underwent a relatively complete dehydration process and was mainly transformed into hemihydrate gypsum (bassanite) with high cementitious activity, together with the formation of a certain amount of soluble anhydrite (anhydrite III). This finding is in close agreement with the mechanical property results discussed above, in which the sample modified at 200°C exhibited the highest 2 h flexural and compressive strengths. As the principal active phase responsible for strength development in gypsum-based materials, the marked increase in hemihydrate gypsum content directly led to the peak in early mechanical performance.

When the temperature was further increased to 220°C, the phase composition evolved again. Additional diffraction peaks associated with more complex calcium sulfate hydrate phases appeared, while the peaks of bassanite and anhydrite were still retained. This phenomenon may suggest that, at excessively high temperatures, part of the gypsum underwent more complex solid-state reactions or structural reorganization, resulting in the formation of relatively stable secondary phases. The cementitious activity of such phases is generally lower than that of hemihydrate gypsum. From the perspective of phase composition, this provides a reasonable explanation for the decline in early strength observed in the sample treated at 220°C: excessively high temperature reduced or transformed the beneficial active phase, namely hemihydrate gypsum, and may also have promoted the formation of new phases unfavorable to cementitious performance.

Overall, the results demonstrate that the modification temperature determined the final phase composition of waste gypsum by controlling its dehydration and phase transformation pathways. Previous studies have shown that gypsum undergoes a continuous transformation from the dihydrate phase to the hemihydrate phase and then to soluble anhydrite within the approximate temperature range of 100–200°C, while temperatures around 190–200°C are often associated with a relatively high hemihydrate gypsum content and superior early mechanical properties [43]. The XRD results provide direct crystallographic evidence for the differences in mechanical performance of waste gypsum treated at different temperatures and clearly identify 200°C as the most suitable modification temperature for achieving efficient cementitious activation of waste gypsum.

3.4 Thermal analysis and chemical characterization

3.4.1 TG-DSC

The TG-DSC analysis shown in Figure 10 was performed on the untreated waste gypsum raw material before thermal modification. As shown in Figure 10, the untreated waste gypsum exhibited two main stages of mass loss during heating from 30 to 250°C. The first slight mass loss was approximately 0.55%, which can be attributed mainly to the evaporation of physically adsorbed water and weakly bound water. The second and more pronounced mass loss was approximately 6.39%, occurring mainly within the temperature range of 80–150°C. This stage was associated with the dehydration of calcium sulfate dihydrate and the formation of hemihydrate gypsum and/or partially dehydrated calcium sulfate phases. Therefore, the dehydration-related thermal response of the untreated waste gypsum was concentrated mainly within 80–150°C. It should be noted that the total measured mass loss was approximately 6.94%–6.95% based on Figure 10, which is much lower than the theoretical water loss of pure gypsum during conversion from dihydrate gypsum to hemihydrate gypsum, approximately 15.7%, or during complete dehydration to anhydrite, approximately 20.9%. This difference indicates that the untreated waste gypsum used in the TG-DSC test was not pure dihydrate gypsum. Instead, it likely contained non-gypsum impurities, inert mineral components, and/or calcium sulfate phases with lower water content [41, 42].

When the temperature exceeded 150°C, the TG curve gradually plateaued, and the sample mass remained nearly constant. Meanwhile, no new pronounced endothermic or exothermic peaks appeared on the DSC curve, indicating that, within the experimental temperature range investigated here (≤250°C), the major dehydration process of gypsum had been essentially completed and no

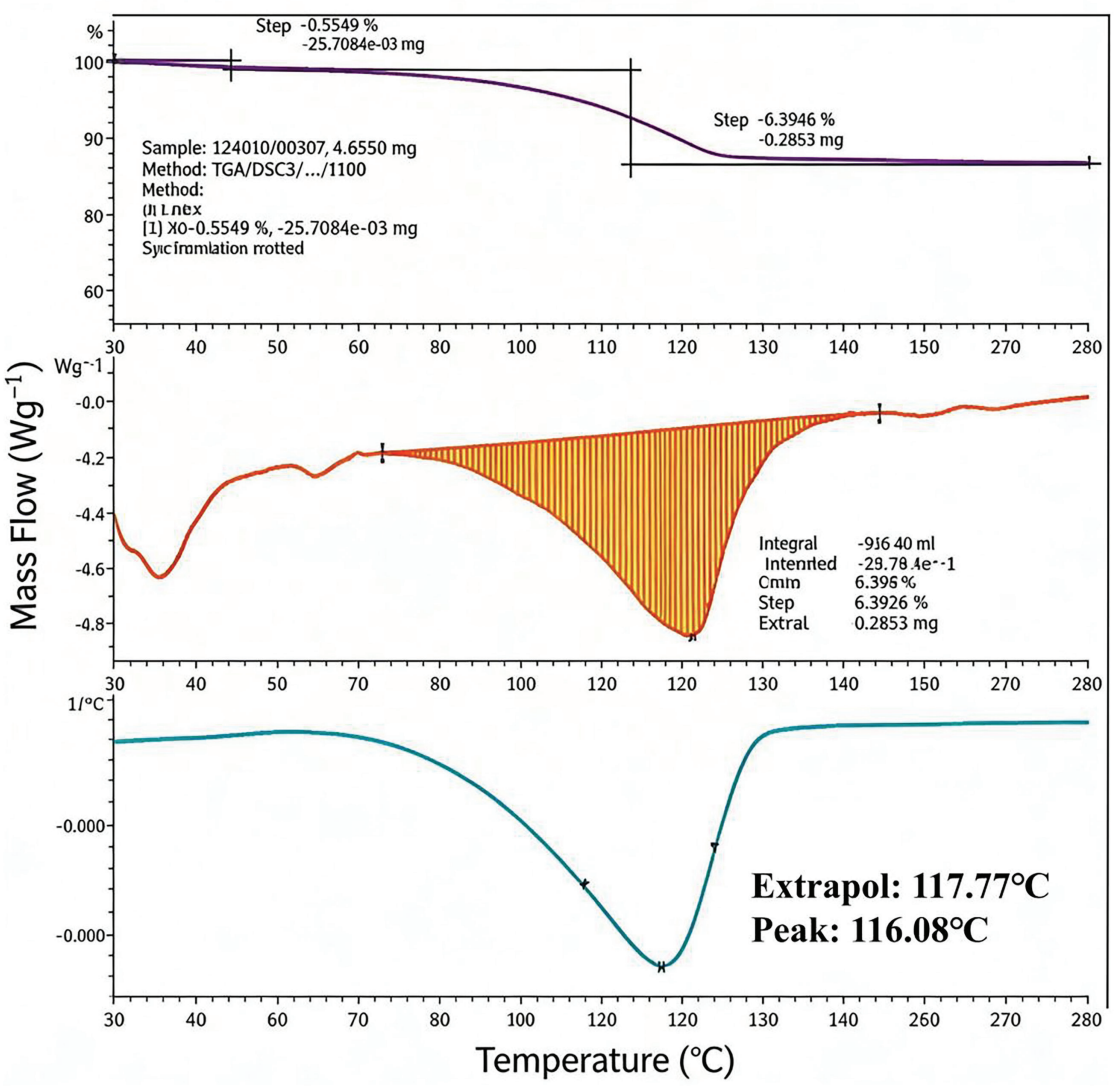


Figure 10 TG-DSC curves of the untreated waste gypsum raw material

further significant phase transformation occurred. This suggests that thermal modification at around 200°C is sufficient to promote the conversion of gypsum into hemihydrate gypsum with relatively high cementitious activity, without generating large amounts of insoluble anhydrite II.

Overall, the TG-DSC results indicate that the critical temperature range for dehydration and phase transformation of the waste gypsum was concentrated within 100–150°C, and that approximately 120°C can be regarded as the characteristic temperature for the conversion of gypsum to hemihydrate gypsum. This conclusion is in close agreement with the XRD phase analysis and mechanical property results discussed above, and further verifies from a thermal analysis perspective that waste gypsum modified at 200°C can achieve a relatively high hemihydrate gypsum content and excellent early strength. Therefore, the TG-DSC analysis provides thermodynamic support for the rationality of the selected thermal modification parameters.

3.4.2 FTIR

To further examine how thermal treatment at different temperatures influenced the functional-group characteristics of waste gypsum, Fourier transform infrared spectroscopy (FTIR) was conducted on samples treated at 160, 180, 200, and 220°C, and the corresponding spectra are presented in Figure 11.

The overall spectra show that the main infrared absorption bands appeared at nearly the same positions for all thermally treated samples, suggesting that the fundamental chemical framework of the gypsum was not substantially altered by thermal modification and that the material still mainly consisted of a calcium sulfate system. Nevertheless, noticeable variations were found in the intensity and sharpness of the characteristic bands, indicating changes in the hydration state of the material and the extent of gypsum dehydration.

The broad band in the region of 3550–3620 cm^{-1} is generally associated with vibrations

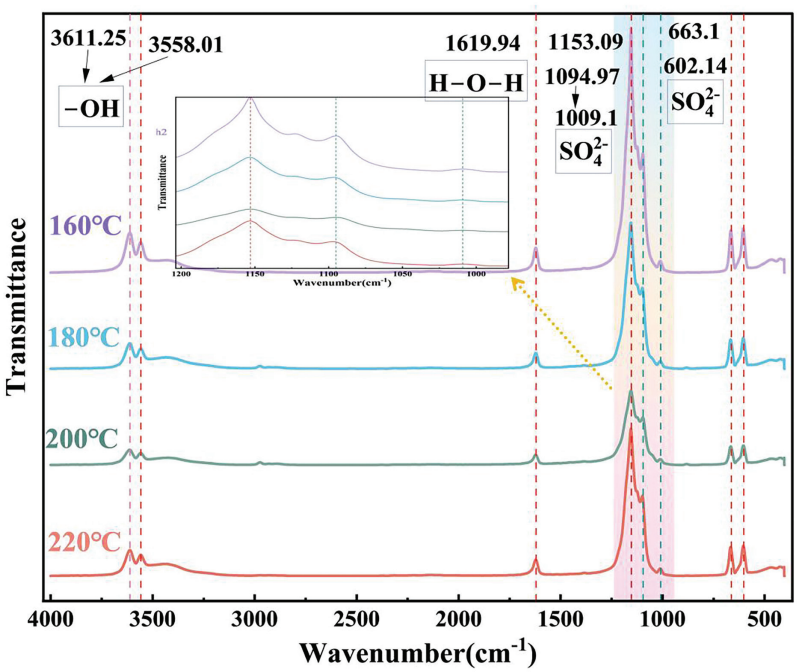


Figure 11 FTIR detection results

of crystallization water and hydroxyl groups [41]. In particular, the samples treated at 160 and 180°C exhibited relatively strong absorption bands at 3558–3612 cm^{-1}, indicating that a considerable amount of crystallization water was still retained in the samples and that the characteristics of gypsum remained evident. As the modification temperature increased to 200°C, the intensity of this band decreased markedly, suggesting that part of the crystallization water had been removed from the crystal structure and that gypsum was gradually transformed into hemihydrate gypsum (bassanite). This trend is highly consistent with the main dehydration interval identified by the TG-DSC analysis.

The absorption bands near 1094–1097 cm^{-1} and 600–670 cm^{-1} can be assigned to the characteristic vibrations of the sulfate group (SO_4^{2-}) [41], further confirming the change in the water state of the samples. As the temperature increased from 160 to 200°C, the intensity of these bands gradually changed, indicating the continuous progress of the dehydration reaction.

A strong absorption band was observed at 1094–1097 cm^{-1} in all samples, corresponding to the asymmetric stretching vibration of the S-O bond in SO_4^{2-}, which is a typical characteristic band of calcium sulfate materials. This band was sharpest and most concentrated in the sample treated at 200°C, indicating that the gypsum crystal structure was more ordered and that the coordination environment of sulfate groups was relatively stable under this condition. This observation is in good agreement with the more regular crystal morphology observed by SEM and the enhanced diffraction peaks of hemihydrate gypsum identified by XRD.

In addition, distinct absorption bands were observed at 663 cm^{-1} and 601–602 cm^{-1}, corresponding to the bending vibrations of SO_4^{2-}. With increasing modification temperature, the positions of these bands remained essentially unchanged; however, the band shapes became clearer in the sample treated at 200°C, suggesting that the calcium sulfate lattice structure was more well developed under this condition, which is beneficial for subsequent hydration and strength development.

When the modification temperature was further increased to 220°C, the absorption band associated with –OH showed a slight increase, while some sulfate-related characteristic bands became somewhat dispersed. This increase in the –OH band may initially appear to contradict the concept of "excessive dehydration" at 220°C. However, this phenomenon can be explained by the enhanced hygroscopicity of the soluble anhydrite III (AIII) phase formed at this temperature. AIII possesses a highly defective, porous structure that readily adsorbs moisture from the ambient atmosphere during sample cooling, handling, and FTIR measurement. This adsorbed water is physically bound surface water, not structural crystallization water. Therefore, the increase in the –OH band does not indicate a higher degree of hydration; rather, it reflects the moisture adsorption capacity of the AIII-rich sample. The loss of crystalline water (i.e., excessive dehydration) is independently confirmed by the XRD results (Section 3.3), which show the transformation of hemihydrate into AIII, and by the decline in mechanical properties at 220°C (Section 3.1.1).

Overall, the FTIR results indicate that thermal modification mainly altered the hydration state and calcium sulfate crystal structure of waste

gypsum by regulating the degree of removal of crystallization water. In the 160–180°C range, dehydration remained incomplete and the characteristics of gypsum were still evident. At 200°C, the features of hemihydrate gypsum were the most pronounced, and the crystal structure appeared relatively stable and ordered, making this the most favorable temperature range for achieving high cementitious activity. In contrast, treatment at 220°C may have been unfavorable for early mechanical strength development because of excessive dehydration. The slight increase in the –OH band at 220°C is attributed to surface-adsorbed moisture on the hygroscopic AIII phase, which is consistent with rather than contradictory to the occurrence of excessive dehydration. Therefore, the FTIR results further confirm at the functional-group level that 200°C was the optimum thermal modification condition for waste gypsum, in good agreement with the conclusions drawn from the TG-DSC, XRD, and mechanical property analyses.

3.4.3 XRF

To further evaluate the effect of thermal modification on the chemical composition of waste gypsum, XRF analysis was carried out for the blank sample and the samples treated at 160, 180, 200, and 220°C (Figure 12 and Table 2). The results show that SO_3 and CaO were the dominant components in all samples, confirming that the material was mainly composed of calcium sulfate-based phases. After thermal modification, the SO_3 content remained within the range of 64.132%–65.351%, while the CaO content varied only slightly between 34.240% and 35.612%, indicating that the main chemical composition of the gypsum remained essentially stable during heating. This result suggests that thermal modification primarily changed the hydration state and phase composition of the material rather than altering its fundamental chemical framework.

Compared with the blank sample, the contents of minor oxides such as SiO_2, Fe_2O_3, SrO, K_2O, and CuO were all low, and most of them showed a decreasing trend after thermal treatment. In particular, SiO_2 decreased from 0.980% in the blank sample to 0.167%–0.202% in the modified samples, and Fe_2O_3 decreased from 0.151% to 0.013%–0.055%. These changes may be related to the redistribution effect caused by dehydration and the increased relative proportion of calcium sulfate phases after calcination. In addition, Al_2O_3 was detected only in the blank sample, whereas it was not detected in the modified samples, suggesting that its content was extremely low after heat treatment or below the detection limit of the instrument.

Overall, the XRF results indicate that thermal modification at 160–220°C did not fundamentally change the chemical composition of the waste gypsum, but mainly promoted dehydration and phase transformation within the Ca-S-O system. This conclusion is consistent with the XRD, FTIR, and TG-DSC results, which together demonstrate that the improvement in mechanical properties was mainly associated with phase evolution and microstructural optimization rather than with changes in bulk chemical composition.

3.5 Analysis of the mechanism of temperature modification

The strength enhancement of the modified waste gypsum can be further explained by the combined effects of phase transformation and internal structural optimization. During thermal treatment, part of the dihydrate gypsum was dehydrated to hemihydrate gypsum and soluble anhydrite, which are more reactive during subsequent hydration. Upon mixing with water, these active calcium sulfate phases can rapidly rehydrate and generate newly formed dihydrate gypsum crystals. The intergrowth and overlapping of hydration products contribute to the formation of a more

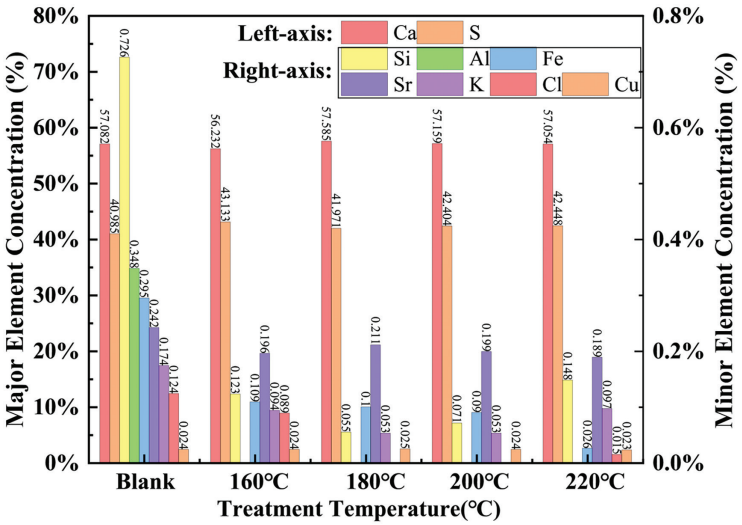


Figure 12 Element concentration

Table 2 Oxide composition

Oxide	Groups					Unit
	Blank	160°C	180°C	200°C	220°C	
SO_3	62.683	65.351	64.132	64.592	64.606	%
CaO	35.466	34.24	35.612	35.142	35.031	%
SiO_2	0.98	0.167	0.088	0.097	0.202	%
Al_2O_3	0.463	n.d.	n.d.	n.d.	n.d.	%
Fe_2O_3	0.151	0.055	0.052	0.03	0.013	%
SrO	0.102	0.08	0.075	0.082	0.078	%
K_2O	0.102	0.053	0.03	0.046	0.055	%
Cl	0.041	0.043	n.d.	n.d.	0.01	%
CuO	0.012	0.011	0.011	0.011	0.005	%

compact hardened matrix, thereby improving the load-bearing capacity of the material.

This interpretation is supported by the phase-composition and XRD results, which indicate that the treatment at 200°C promoted the formation of hemihydrate gypsum while avoiding excessive transformation into less reactive anhydrite phases. In addition, the PSD results suggest that the 200°C-treated sample had a relatively favorable particle/agglomerate distribution, which may improve particle packing and reduce structural defects in the hardened body. Therefore, the improvement in flexural and compressive strength at 200°C, especially after 6 h of treatment, can be attributed not only to the increase in reactive gypsum phases but also to the development of a denser and more continuous internal structure. In contrast, excessive heating at 220°C may lead to over-dehydration, local agglomeration, or the formation of less favorable calcium sulfate phases, thereby weakening the structural compactness and limiting further strength development.

The thermal modification of waste gypsum mainly involves a series of processes, including dehydration, crystal structure reconstruction, and microstructural optimization. As illustrated in the proposed mechanism diagram (Figure 13), the original waste gypsum existed predominantly in the form of gypsum ($CaSO_4 \cdot 2H_2O$). Its crystal structure contained a large amount of crystallization water, and the crystal morphology was relatively loose. At the same time, a certain amount of impurity elements, such as Cu, As, and Pb, were distributed on the crystal surfaces or within the intercrystalline spaces.

Under thermal treatment, the waste gypsum first underwent a dehydration process. As the temperature increased to an appropriate range, gypsum gradually lost part of its crystallization water and was transformed into hemihydrate gypsum ($CaSO_4 \cdot 0.5H_2O$). With a further increase in temperature, part of the hemihydrate gypsum could continue to dehydrate and form anhydrite ($CaSO_4$). This process was accompanied by a rearrangement of the crystal structure, through which the originally loose crystals gradually evolved into a more regular and stable configuration. Meanwhile, the pore structure within the gypsum particles was also altered during heat treatment. Some micropores shrank or were redistributed under elevated temperature, leading to a denser overall structure of the material. In addition, thermal modification promoted renewed bonding and intergrowth between crystals, resulting in the formation of a more stable interlocking crystal structure. Such an interwoven crystal network can effectively enhance the structural stability and mechanical performance of the material.

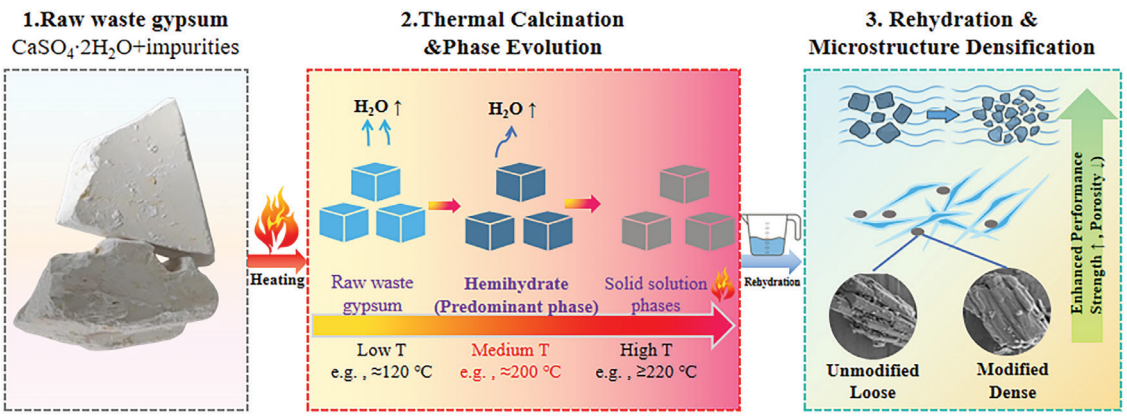


Figure 13 Mechanism diagram of temperature modification

On the other hand, thermal modification may also affect the occurrence state of heavy metal elements in waste gypsum. During heat treatment, some heavy metals may be stabilized within the gypsum structure through physical encapsulation, lattice fixation, or association with mineral phases, thereby reducing their mobility and potential environmental risk. These mechanistic interpretations are consistent with the general behavior of gypsum during thermal dehydration, crystal reconstruction, and subsequent rehydration hardening [17, 24, 40, 42].

In addition, the particle size distribution and XRF results indicate that thermal modification not only affected particle characteristics and packing behavior, but also maintained the overall chemical stability of the Ca-S-O framework. Therefore, the improvement in mechanical performance was mainly governed by dehydration-induced phase transformation, particle redistribution, and microstructural densification rather than by any substantial change in elemental composition.

3.6 Heavy metal testing and analysis

To assess the environmental safety of waste gypsum for resource utilization, the concentrations of several common heavy metals in the modified gypsum samples were measured by ICP-MS. Particular focus was placed on Cu, As, Cd, Hg, and Pb because these elements may pose potential environmental concerns. The corresponding results are listed in Table 3. Overall, the measured concentrations of these heavy metals in the waste gypsum were low. Specifically, Cu, As, and Pb were detected at 0.1766, 0.1893, and 0.2163 mg/kg, respectively, which were all far below the limit values specified in relevant standards for building materials and general solid wastes. The concentrations of Cd and Hg were even lower, reaching only 0.00254 and 0.0648 mg/kg, respectively. These findings indicate that the waste gypsum used in this work did not exhibit significant heavy metal contamination and met the basic environmental safety requirements for resource utilization.

3.7 Carbon emission analysis

In addition to phase transformation, mechanical performance, and environmental safety, the carbon burden of the thermal modification process was also evaluated. Under the optimum treatment condition identified in this study, namely 200°C for 6 h, the modified waste gypsum reached a 2 h compressive strength of 6.0 MPa. To assess the process-related carbon emission of this condition, the electricity consumption of the electric drying oven was calculated based on its rated power of 2.2 kW and the treatment duration of 6 h. The resulting electricity consumption for one batch was 13.2 kWh.

Table 3 **Heavy metal testing results**

Test element	Elemental content of the sample Cx (mg/kg)
Cu	0.1766
As	0.1893
Cd	0.002538
Hg	0.06480
Pb	0.2163

The electricity consumption for thermal modification was estimated using the rated power of the oven rather than directly measured power consumption. Specifically, the calculation assumed that the oven operated continuously at its rated power of 2.2 kW throughout the 6 h holding period, The associated carbon emissions were then calculated using the selected electricity-emission factor. This approach provides a simplified rated-power-based estimate for comparing the carbon-emission performance of different treatment conditions. In actual operation, however, the oven temperature is controlled thermostatically after reaching the set temperature, and the heating elements cycle on and off. Therefore, the actual average power draw during the holding stage may be lower than the rated power. As a result, the reported electricity consumption, carbon emissions, and energy-efficiency indicators should be interpreted as estimated values under a full-rated-power assumption, rather than as directly measured operational values. Future work should employ electricity metering to obtain the actual energy consumption of the thermal-modification process.

Using the 2024 national average electricity carbon footprint factor of 0.5777 kg CO_2-eq/kWh [44], the process carbon emission of one heating batch was calculated as follows Eq. (9):

$$CF = 2.2 \times 6 \times 0.5777 = 7.63\,kg\,CO_2\text{-eq} \quad (9)$$

Since 2 kg of waste gypsum was treated in each batch, the corresponding unit carbon emission was Eq. (10):

$$CF_{unit} = 7.63/.81kg\ CO_2 - eq/kg \quad (10)$$

Furthermore, based on the compressive strength of 6.0 MPa for the optimum sample, the carbon efficiency was determined as Eq. (11):

$$CE = 6.0/3.81 = 1.57 \quad (11)$$

These results (Figure 14) indicate that the optimum thermal modification condition of 200°C for 6 h produced a process carbon emission of 7.63 kg CO_2-eq per batch and a unit carbon emission of 3.81 kg CO_2-eq/kg, while maintaining satisfactory mechanical performance. The impact of thermal modification on the carbon efficiency index is the result of a trade-off between 'strength enhancement' and 'carbon emissions'. In this study, compressive strength was increased to 6 MPa, but carbon emissions per unit increased from 0 to 3.81 kg CO_2-eq/kg, resulting in additional carbon dioxide emissions. This does not negate the value

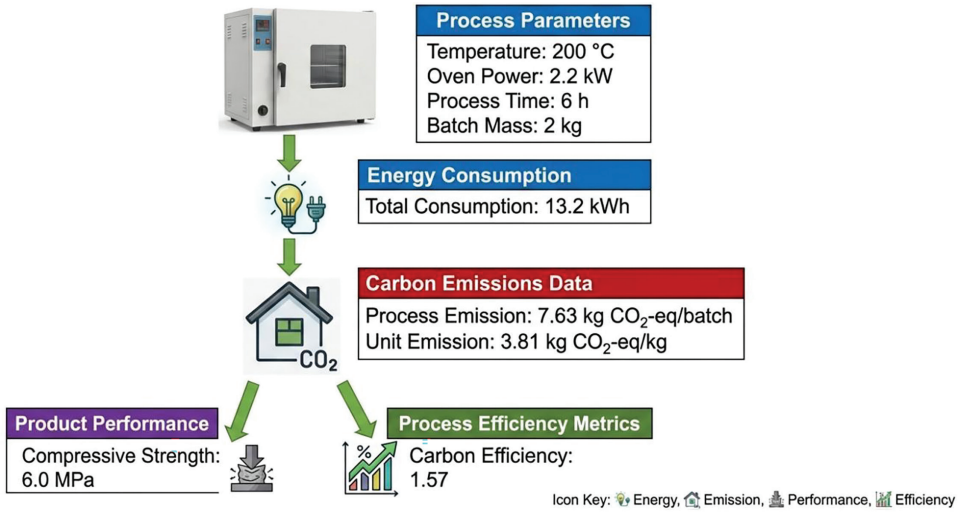


Figure 14 Estimated carbon emissions and energy-efficiency indicators for thermal modification under the rated-power assumption

of thermal modification, but rather highlights its specific application context: thermal modification is an activation method characterised by 'high carbon costs and high-performance outputs', suitable for building materials where there are specific strength requirements.

From the perspective of performance–carbon balance, the carbon efficiency index provides a useful indicator for evaluating the environmental rationality of the modification process. In the present study, the carbon efficiency of the optimum sample was 1.57, indicating that the selected treatment condition achieved a reasonable balance between strength development and carbon burden. Future process optimization should focus on reducing carbon emissions while maintaining strength gains by lowering heat treatment temperatures or durations, utilizing waste heat, or combining with low-carbon cementitious materials, ultimately enhancing carbon efficiency.

It should be emphasized that the environmental assessment performed in this study differs from previous investigations of phosphogypsum-based composite cementitious systems. For example, Wang et al. [32] investigated red-mud-modified phosphogypsum containing several solid-waste and cementitious components, with emphasis on mixture optimization and the environmental risks of heavy metals. In the present study, the starting material is end-of-life industrial mold gypsum, and thermal dehydration is used as the principal regeneration route without introducing additional cementitious solid wastes. Consequently, the environmental burden considered here is directly associated with the thermal regeneration process itself. By relating the treatment-dependent phase evolution and mechanical recovery to process-related carbon emissions and heavy-metal safety, the present results provide a process-specific assessment for the direct recycling of industrial waste mold gypsum.

3.8 Analysis of heavy metal risk assessment

Although five heavy metals, including Cu, As, Pb, Cd, and Hg, were measured in Table 3, only Cu, As, and Pb were carried forward into the subsequent risk-assessment calculations. This selection was based on the measured concentration levels and data validity for the present samples. Cu, As, and Pb were detected at quantifiable levels and therefore provided meaningful input values for the geo-accumulation index, potential ecological risk index, health risk assessment, and carcinogenic/non-carcinogenic risk assessment. In contrast, Cd and Hg were not included in the subsequent quantitative risk calculations because their measured concentrations were extremely low and/or below the effective quantification level, making their calculated risk contributions negligible or unreliable. Therefore, the following risk-assessment section focuses on Cu, As, and Pb as the representative heavy metals with quantifiable concentrations in the tested waste gypsum samples.

3.8.1 Single factor index method

According to the single-factor pollution index results presented in Table 4, the pollution indices of Cu, As, and Pb in the waste gypsum sample were 0.003532, 0.006310, and 0.003090, respectively. The single-factor pollution index (P_i) is calculated as the ratio of the measured concentration of a given heavy metal in the sample to its corresponding reference standard value, and is commonly used to evaluate the environmental impact of an individual pollutant. In general,

Table 4 Calculation results

Cu	As	Pb
0.003532	0.006310	0.003090

a value of P_i < 1 indicates that the element does not pose a significant pollution risk to the environment.

The calculated results show that the pollution indices of all three heavy metals were far below 1, and even lower than 0.01, indicating that the actual concentrations of Cu, As, and Pb in the waste gypsum were substantially lower than the corresponding environmental risk control limits and remained at an extremely low level overall. Among these elements, the pollution index of As was slightly higher than those of Cu and Pb; however, its value was still within an extremely low range, suggesting that its environmental impact can be considered negligible.

3.8.2 Potential ecological risk index

The calculation results (Figure 15a) show that the potential ecological risk indices of all investigated heavy metal elements were at low levels, indicating that the overall ecological risk of the waste gypsum sample can be classified as low. Among these elements, As exhibited a relatively higher potential ecological risk index because of its higher toxic-response coefficient; however, its value was still far below the warning threshold for ecological risk assessment. The potential ecological risk indices of Pb and Cu were even lower, indicating that their potential impacts on the ecological environment were weak.

3.8.3 Geoaccumulation index method

According to the calculation results shown in Figure 15b, the geoaccumulation indices (Igeo) of all investigated heavy metals were below 0, indicating that the waste gypsum sample should be classified as unpolluted from the perspective of geoaccumulation assessment. Among these elements, As showed a slightly higher geoaccumulation index than the others, but its value still remained within the unpolluted range, suggesting that although As was present in the sample, no obvious enrichment had occurred. The geoaccumulation indices of Pb and Cu were even lower, further indicating that their contents were mainly associated with the natural background rather than anthropogenic contamination.

3.8.4 Human health risk assessment

The heavy metal test results indicated that As and Pb occurred at relatively higher levels than the other analyzed elements. Therefore, together with Cu, these elements were selected for subsequent ecological and human health risk evaluation. Multiple assessment approaches were then applied to examine their possible effects on the ecological environment and human health.

As shown in Figure 16, the non-carcinogenic risk indices of all investigated heavy metals were far below 1, indicating that, at their current concentrations, these heavy metals would not pose significant non-carcinogenic risks to human health. Meanwhile, the carcinogenic risk indices were all lower than the safety threshold of 10^{-6}, suggesting that the heavy metal elements present in the waste gypsum would not cause significant carcinogenic risks to humans under normal utilization conditions.

Among the different exposure pathways, oral ingestion contributed relatively more to the overall human health risk; however, the total risk remained within the acceptable safety range. In contrast, the risks associated with inhalation and dermal contact were even lower. Overall, the results indicate that the heavy metal contents in the waste gypsum were low and that their potential hazard to human health was limited. Therefore, from the perspective of human health safety, the waste gypsum material used in this study satisfies the environmental safety requirements for resource utilization and can be reasonably applied in the field of building materials.

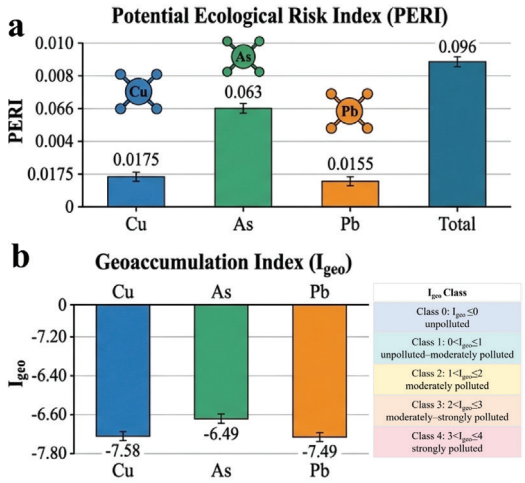


Figure 15 Risk assessment results: (a) Potential Ecological Risk Index; (b) Geoaccumulation index

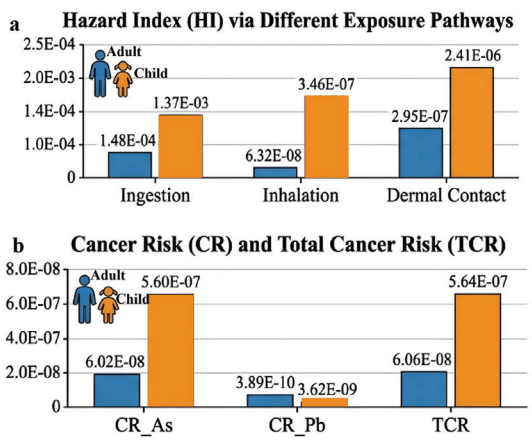


Figure 16 Risk assessment results: (a) Hazard index via different exposure pathways; (b) Cancer risk and total cancer risk

3.9 Circularity and sustainability assessment perspective

In addition to conventional performance evaluation, recent studies have highlighted the importance of circularity-based assessment approaches in sustainable construction and materials research. These methodologies extend traditional environmental and mechanical analyses by incorporating material circularity indicators, resource efficiency, and life-cycle perspectives, thereby providing a more integrated view of material sustainability within a circular economy framework [45, 46]. Although a quantitative circularity assessment is not the focus of this study, the phase transformation behavior and performance evolution of waste gypsum reported here can provide useful input parameters for future circularity modeling and sustainability evaluation of gypsum-based materials.

4 Conclusions

(1) Thermal modification significantly affected the mechanical properties of waste gypsum. Within the temperature range of 160–200°C, the 2 h flexural strength and compressive strength of waste gypsum gradually increased with increasing modification temperature and reached their maximum values at 200°C. When the temperature was further raised to 220°C, the early strength decreased, indicating that excessively high temperature was unfavorable for the development of material performance. The optimum modification condition was determined to be 200°C for 6 h, under which the modified waste gypsum exhibited a 2 h flexural strength of 2.8 MPa and a compressive strength of 6.0 MPa.

(2) XRD and three-phase analysis demonstrated that thermal modification induced phase transformation primarily by regulating the dehydration process of gypsum. In the temperature range of 160–180°C, dehydration remained incomplete and the phase composition was relatively complex. At 200°C, gypsum was largely converted into hemihydrate gypsum, accompanied by the formation of a substantial amount of soluble anhydrite (AIII, 29.2%), representing the critical temperature range for achieving high cementitious activity. SEM-EDS analysis further showed that thermal modification significantly altered the microstructure of waste gypsum. At 200°C, the sample exhibited a more regular crystal morphology, closer particle packing, and a denser microstructure, which contributed to the enhancement of mechanical properties.

(3) TG-DSC, FTIR, and XRF results indicated that the main dehydration reaction of waste gypsum occurred within the range of 100–150°C, with approximately 120°C identified as the characteristic temperature for the conversion of gypsum to hemihydrate gypsum. Modification at 200°C was sufficient to remove crystallization water effectively and to form a stable hemihydrate gypsum structure, thereby improving the cementitious activity of the material. XRF analysis further confirmed that thermal modification mainly affected the hydration state and phase composition of gypsum, while the bulk chemical composition remained essentially stable and continued to be dominated by the Ca-S-O system.

(4) Heavy metal analysis together with risk assessment results indicated that Cu, As, Cd, Hg, and Pb were present at relatively low concentrations in the waste gypsum. In addition, the calculated single-factor pollution index, potential ecological risk index, and human health risk index were all well below the corresponding safety limits. These findings demonstrate that the reutilization of this material is unlikely to cause notable adverse effects on either the ecological environment or human health. Carbon emission assessment showed that the optimum thermal treatment condition of 200°C for 6 h resulted in a process carbon emission of 7.63 kg CO_2-eq per batch and a unit carbon emission of 3.81 kg CO_2-eq/kg. Combined with the corresponding compressive strength of 6.0 MPa, the calculated carbon efficiency reached 1.57, confirming that this condition achieved a reasonable balance between strength enhancement and environmental cost.

Acknowledgement

Not applicable.

Funding Statement

Chongqing Municipal Natural Science Foundation General Program (CSTB2025NSCQ-GPX0844).

Author Contributions

Zhong-jie Wang: Experiments, data analysis, drafting and revising the manuscript. Lian-xing Wang: Resource and project management. Chao-qiang Wang: Experimental design, resources, supervisor, and financial support. All authors reviewed and approved the final version of the manuscript.

Availability of Data and Materials

Data available within the article.

Ethics Approval

Not applicable.

Conflicts of Interest

The authors declare no conflicts of interest.

REFERENCES

[1] Alyousef R, Abbass W, Aslam F, Shah MI. Potential of waste woven polypropylene fiber and textile mesh for production of gypsum-based composite. Case Stud Constr Mater. 2023;18(9):e02099. doi:10.1016/j.cscm.2023.e02099.
[2] Zhi Z, Guo Y, Liu Q, Jin Z, Dong B, Ru X, et al. Surface modification and dispersity of chopped carbon fiber and its effects on mechanical properties of gypsum-based composite materials. Compos Interfaces. 2024;31(2):195–213. doi:10.1080/09276440.2023.2246759.
[3] Jhony de Araújo Silva K, de Vasconcelos Ferraz A. Study of the reuse of gypsum waste in the calcination process of gypsum ore. Mat Res. 2025;28(suppl 1):e20250004. doi:10.1590/1980-5373-mr-2025-0004.
[4] Capasso I, Boccarusso L, Pappalardo L, Iucolano F. Sustainable lightweight gypsum from recycled waste: microstructure and performance. Constr Build Mater. 2025;496:143698. doi:10.1016/j.conbuildmat.2025.143698.
[5] Kang CU, Ji SW, Jo H. Recycling of industrial waste gypsum using mineral carbonation. Sustainability. 2022;14(8):4436. doi:10.3390/su14084436.
[6] Amine Laadila M, LeBihan Y, Caron RF, Vaneeckhaute C. Construction, renovation and demolition (CRD) wastes contaminated by gypsum residues: characterization, treatment and valorization. Waste Manag. 2021;120:125–35. doi:10.1016/j.wasman.2020.11.031.
[7] Villoria Sáez P, del Río Merino M, Atanes Sánchez E, Santa Cruz Astorqui J, Porras-Amores C. Viability of gypsum composites with addition of glass waste for applications in construction. J Mater Civ Eng. 2019;31(3):04018403. doi:10.1061/(asce)mt.1943-5533.0002604.
[8] Gázquez MJ, Bolívar JP, Vaca F, García-Tenorio R, Mena-Nieto A. Use of the "red gypsum" industrial waste as substitute of natural gypsum for commercial cements manufacturing. Mater Constr. 2012;62(306):183–98. doi:10.3989/mc.2011.63910.
[9] Ma X, Tan L, Lu Y, Yao W, Wei Y. Upcycling of waste plasterboard for the synthesis of high-quality gypsum-based 3D printing powder. Constr Build Mater. 2023;373(2):130846. doi:10.1016/j.conbuildmat.2023.130846.
[10] Liu Y, Zhang Y, Guo Y, Chu PK, Tu S. Porous materials composed of flue gas desulfurization gypsum and textile fiber wastes. Waste Biomass Valorization. 2017;8(1):203–7. doi:10.1007/s12649-016-9617-y.
[11] Zhu C, Zhang J, Yi W, Cao W, Peng J, Liu J. Research on degradation mechanisms of recycled building gypsum. Constr Build Mater. 2018;173:540–9. doi:10.1016/j.conbuildmat.2018.04.060.
[12] Wang S, Lin X, Wang C. Dual benefits of indirect mineral carbonation of titanium gypsum: waste gypsum recycling and carbon sequestration. Environ Res. 2025;285(Pt 2):122393. doi:10.1016/j.envres.2025.122393.
[13] Pu S, Zhu Z, Huo W. Evaluation of engineering properties and environmental effect of recycled gypsum stabilized soil in geotechnical engineering: a comprehensive review. Resour Conserv Recycl. 2021;174(1):105780. doi:10.1016/j.resconrec.2021.105780.
[14] Dai X, Zhang Y, Ye J, Liu C, Liu Z. Effect of β-hemihydrate gypsum on the properties of γ-C2S slurry before and after carbonation. Buildings. 2026;16(4):799. doi:10.3390/buildings16040799.
[15] Jin Z, Ma B, Su Y, Qi H, Lu W, Zhang T. Preparation of eco-friendly lightweight gypsum: use of beta-hemihydrate phosphogypsum and expanded polystyrene particles. Constr Build Mater. 2021;297(6):123837. doi:10.1016/j.conbuildmat.2021.123837.
[16] Lu M, Ma W, Guo Z, Shi Y, Liu M, Zhang H. Controlling impurity effects in phosphogypsum calcination: a combined regression and DFT study for optimizing β-hemihydrate gypsum production. Mater Res Express. 2025;12(7):075501. doi:10.1088/2053-1591/ade496.
[17] Zhang L, Mo KH, Tan TH, Hung CC, Yap SP, Ling TC. Influence of calcination and GGBS addition in preparing β-hemihydrate synthetic gypsum from phosphogypsum. Case Stud Constr Mater. 2023;19(4):e02259. doi:10.1016/j.cscm.2023.e02259.
[18] Rahaman MN. Ceramic processing. Boca Raton, FL, USA: CRC Press; 2017.
[19] Nejatian T, Firouzmanesh P, Yaqin Syed AU. Dental gypsum and investments. In: Advanced dental biomaterials. Amsterdam, The Netherlands: Elsevier; 2019. p. 37–54. doi:10.1016/b978-0-08-102476-8.00003-7.
[20] Kryuchkov YN, Neklyudova TL. Structure of gypsum and polymer molds for slip casting. Glass Ceram. 2015;71(9):324–6. doi:10.1007/s10717-015-9679-5.
[21] Ochoa RE, Gutiérrez CA, López-Cuevas J, Rendón J, Rodríguez-Galicia JL, Cruz-Álvarez J. Effect of water/plaster ratio on preparing molds for slip casting of sanitaryware; rheology of the initial plaster slurry, microstructure and mold properties. Trans Indian Ceram Soc. 2018;77(2):84–9. doi:10.1080/0371750x.2018.1475262.
[22] Geraldo RH, Pinheiro SMM, Silva JS, Andrade HMC, Dweck J, Gonçalves JP, et al. Gypsum plaster waste recycling: a potential environmental and industrial solution. J Clean Prod. 2017;164(2):288–300. doi:10.1016/j.jclepro.2017.06.188.
[23] Lazar L, Balasanian I. Valorization of plaster molds waste from fine ceramic industry. Environ Eng Manag J. 2010;9(1):141–6. doi:10.30638/eemj.2010.021.
[24] Krejsová J, Kužel R, Keppert M, Scheinherrová L, Vimmrová A. New insight into the phase changes of gypsum. Mater Struct. 2024;57(5):128. doi:10.1617/s11527-024-02404-z.
[25] Elert K, Bel-Anzué P, Burgos-Ruiz M. Influence of calcination temperature on hydration behavior, strength, and weathering resistance of traditional gypsum plaster. Constr Build Mater. 2023;367(1):130361. doi:10.1016/j.conbuildmat.2023.130361.
[26] Wei Z, Zhang Q, Li X. Crystallization kinetics of α-hemihydrate gypsum prepared by hydrothermal method in atmospheric salt solution medium. Crystals. 2021;11(8):843. doi:10.3390/cryst11080843.
[27] Zhang J, Wang X, Hou P, Jin B, Zhang X, Li Z. Effect of phosphoric acid on the preparation of α-hemihydrate gypsum using hydrothermal method. Materials. 2023;16(17):5878. doi:10.3390/ma16175878.
[28] Liu J, Dong F, Tan H, Zhang H, Zhou L, He P, et al. Facile preparation of high-strength α-$CaSO_4{\cdot}0.5H_2O$ regulated by maleic acid from phosphogypsum: experimental and molecular dynamics simulation studies. SN Appl Sci. 2020;2(10):1645. doi:10.1007/s42452-020-03387-6.
[29] Esan MT. Review of gypsum reinforced composites as building materials. Discover Civ Eng. 2024;1(1):5. doi:10.1007/s44290-024-00005-x.
[30] Pundir A, Garg M, Singh R. Evaluation of properties of gypsum plaster-superplasticizer blends of improved performance. J Build Eng. 2015;4:223–30. doi:10.1016/j.jobe.2015.09.012.
[31] Wang L, Cao M, Li X, Du W, Wang X. A novel approach for improving the water resistance of gypsum plaster by internal mixing hypromellose and external coating waterproofing agent. Constr Build Mater. 2023;401(8):132940. doi:10.1016/j.conbuildmat.2023.132940.
[32] Wang CQ, Chen S, Huang DM, Huang QC, Li XQ, Shui ZH. Safe environmentally friendly reuse of red mud modified phosphogypsum composite cementitious material. Constr Build Mater. 2023;368(11):130348. doi:10.1016/j.conbuildmat.2023.130348.
[33] Pedreño-Rojas MA, Flores-Colen I, De Brito J, Rodríguez-Liñán C. Influence of the heating process on the use of gypsum wastes in plasters: mechanical, thermal and environmental analysis. J Clean Prod. 2019;215(1):444–57. doi:10.1016/j.jclepro.2019.01.053.
[34] Wang CQ, Liu K, Huang DM, Chen Q, Tu MJ, Wu K, et al. Utilization of fly ash as building material admixture: basic properties and heavy metal leaching. Case Stud Constr Mater. 2022;17(2):e01422. doi:10.1016/j.cscm.2022.e01422.
[35] Wang CQ, Chen S, Yang FH, Wang AM. Study on properties of representative ordinary Portland cement: heavy metal risk assessment, leaching release kinetics and hydration coupling mechanism. Constr Build Mater. 2023;385(2):131507. doi:10.1016/j.conbuildmat.2023.131507.
[36] Technical guidelines for risk assessment of soil contamination of land for construction. [cited 2026 Aug 20]. Available from: https://www.mee.gov.cn/ywgz/fgbz/bz/bzwb/trhj/201912/t20191224_749893.shtml.
[37] de Castro Souza E, de Vasconcelos Ferraz A. Study of the conversion of the dihydrate phase into β-hemihydrate from two varieties of the mineral gypsum. Matéria. 2025;30:e20240726. doi:10.1590/1517-7076-rmat-2024-0726.
[38] Standard test methods for physical testing of gypsum, gypsum plasters, and gypsum concrete. 2020 [cited 2026 Aug 20]. Available from: https://store.astm.org/c0472-20.html. ASTM C472-20.
[39] Chen Z, Sucech S, Faber KT. A hierarchical study of the mechanical properties of gypsum. J Mater Sci. 2010;45(16):4444–53. doi:10.1007/s10853-010-4527-z.
[40] Beaugnon F, Preturlan JGD, Fusseis F, Gouillart E, Quiligotti S, Wallez G. From atom level to macroscopic scale: structural mechanism of gypsum dehydration. Solid State Sci. 2022;126(1):106845. doi:10.1016/j.solidstatesciences.2022.106845.
[41] Prasad PSR. Direct formation of the-$CaSO_4$ phase in dehydration process of gypsum: *in situ* FTIR study. Am Mineral. 2005;90(4):672–8. doi:10.2138/am.2005.1742.
[42] Vimmrová A, Krejsová J, Scheinherrová L, Doleželová M, Keppert M. Changes in structure and composition of gypsum paste at elevated temperatures. J Therm Anal Calorim. 2020;142(1):19–28. doi:10.1007/s10973-020-09528-8.
[43] Guo H, Wang Q, Li W, Feng X, Yang J, Cao J, et al. Phase transformation and physical properties of binding materials fabricated from solid waste FGD gypsum by oil bath heating and the micromorphology and formation mechanism of their hydration products. Constr Build Mater. 2023;377(1–2):130981. doi:10.1016/j.conbuildmat.2023.130981.
[44] Announcement on the release of 2024 power carbon footprint factor data. 2025 [cited 2026 Aug 20]. Available from: https://www.mee.gov.cn/xxgk2018/xxgk/xxgk01/202510/t20251024_1130734.html.
[45] Nia SB, Nyland A, Wivast J, Kioumarsi M, Shafei B. Investigations of Portland limestone cement and waste glass powder for sustainable ultra-high performance concrete. Case Stud Constr Mater. 2025;22(1):e04425. doi:10.1016/j.cscm.2025.e04425.
[46] Farahzadi L, Bozorgmehr Nia S, Shafei B, Kioumarsi M. Sustainability assessment of ultra-high performance concrete made with various supplementary cementitious materials. Clean Mater. 2025;15(24):100301. doi:10.1016/j.clema.2025.100301.